Appl Phys A (2008) 93: 495–504
DOI 10.1007/s00339-008-4843-1

Applied Physics A
Materials Science & Processing

RAPID COMMUNICATION

The role of defects in chemical sensing properties of carbon nanotube films

Zsolt E. Horváth · Antal A. Koós · Krisztián Kertész · György Molnár · Gábor Vértesy · Márton C. Bein · Tamás Frigyes · Zoltán Mészáros · József Gyulai · László P. Biró

Received: 18 April 2008 / Accepted: 17 July 2008 / Published online: 8 August 2008

Abstract The electrical resistance of 24 different carbon nanotube (CNT) thin film samples in blowing ambient air and 10 different analyte vapor environments was measured. The effects of the CNT growth method, different chemical treatments, ball milling, sample preparation conditions and Ar^+-ion irradiation are compared. Significant differences in the response signal curves as a function of time in the case of the studied sensor/vapor combinations show the important role of the defect structure and attached functional groups in the chemical sensing properties of CNTs.

PACS 73.63.Fg · 85.35.Kt · 07.07.Df · 68.43.-h · 68.35.Dv

1 Introduction

Carbon nanotubes (CNTs) have attracted great attention due to their extraordinary properties [1]. CNTs have tubular structure with large surface-to-volume ratio [2], which provides plenty of sites for gas molecules to adsorb. The adsorption of gas molecules either donates or withdraws electrons to or from the CNT, leading to changes in the CNT electrical properties [3]. In the case of single-wall CNTs (SWCNTs), all the atoms are surface atoms and, in the case of multiwall CNTs (MWCNTs), the electrical conductance is mainly determined by the surface atoms [4]. This means that there is no need for diffusion, which would increase the response time of the sensor. These factors enable CNTs to be an ideal candidate for gas sensing materials. Another important consequence of the pivotal role of the surface is that the electronic properties of CNTs can be effectively tuned by functionalization [5]. The strong carbon–carbon bonding on the hexagonal network of their side wall makes ideal CNTs relatively inert. However, the change of the local reactivity around structural defects present in real CNT structures makes their interaction with ambient chemical species more probable. Defects, including bends and tube ends, are considered as connecting sites of functional groups and adsorption sites of gas and vapor molecules [5–12].

Both single- and multiwall CNTs used in 'single-tube' devices modified their transport properties due to changes in the ambient [13, 14]. Nevertheless, the single-tube technology is complex and expensive and therefore cannot compete with chemical sensors already on the market. Additionally, these devices have individual characteristics arising from the particular chirality and the tube diameter; therefore, the production of identical devices is extremely demanding. CNT mats behave as random conductive networks; their use as electronic and sensing material seems to be more promising in applications [15]. For example, several groups have reported chemical sensing properties of both SWCNT [16–18] and MWCNT [19, 20] based multitube sensors.

Here we report the fabrication and comparative study of chemical sensing elements made of random networks of Chemical Vapour Deposition (CVD)-grown MWCNTs after different treatments, which modify the degree and type of functionalization and defect density. As a comparison, other SWCNT and MWCNT materials grown by an electric arc

Z.E. Horváth (✉) · A.A. Koós · K. Kertész · G. Molnár · G. Vértesy · M.C. Bein · T. Frigyes · Z. Mészáros · J. Gyulai · L.P. Biró
Research Institute for Technical Physics and Materials Science—MFA, Konkoly Thege Miklós út 29-33, 1121 Budapest, Hungary
e-mail: horvatze@mfa.kfki.hu

M.C. Bein · T. Frigyes · Z. Mészáros
Budapest University of Technology and Economics, Műegyetem rkp. 3-9, 1111 Budapest, Hungary

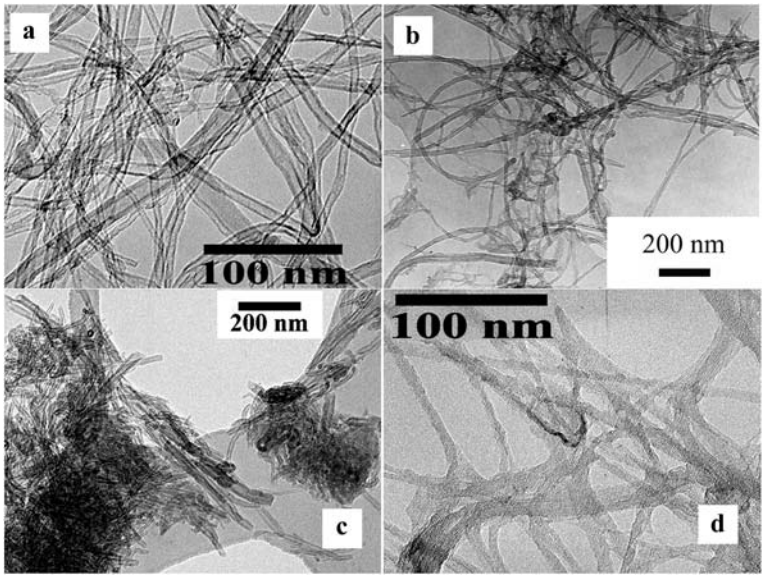

Fig. 1 Characteristic TEM images of four selected carbon nanotube materials: (**a**) G1–CCVD-grown MWCNT, (**b**) G2–CCVD-grown MWCNT, mixed in 3:1 H_2SO_4: HNO_3, $SOCl_2$ and DAP, (**c**) G19–CCVD-grown MWCNT ball milled in Cl_2, (**d**) G12–SWCNT arc-grown in He

method were also studied. We aimed at using simple preparation and quick measuring methods to enable the testing of the response of several different sensors on numerous gases and vapors. The starting CNT material (see Transmission Electron Microscopy (TEM) image in Fig. 1a) was on one hand annealed in high-purity nitrogen at high pressure and temperature in order to remove the functional groups and heal the structural defects. High-temperature annealing was proven to remove the defect sites of raw MWCNTs by Bom et al. [21]. The partial defect healing effect of annealing in nitrogen at as low as 450°C was proven by scanning tunneling microscopy [22]. On the other hand, conventional wet chemical and mechanochemical functionalization methods as well as Ar^+-ion irradiation were applied to reach a higher density of defects [22] and different functional groups on the CNT surfaces.

2 Experimental

The list of the investigated CNT materials and their preparation methods are presented briefly in Table 1. TEM images of four typical samples are shown in Fig. 1. CNTs used for gas sensing experiments were produced by catalytic CVD (CCVD) [23] (materials of G01–G11, G15–G20 and G22–G24) and electric arc discharge [24–26] (materials of G12–G14 and G21). The material of G14 was used in as-prepared form, while all the other materials were purified after production. The materials of G12 and G13 were refluxed in 3M HNO_3 for 45 h. The CCVD MWCNTs were synthesized by catalytic decomposition of acetylene on alumina-supported Co/Fe catalyst and then purified in two steps. First, the alumina support was dissolved by refluxing in sodium hydroxide solution. In the next step, the metal traces were dissolved by stirring the carbon sample in concentrated hydrochloric acid. The two steps were repeated twice in order to remove all catalyst traces. Finally, the MWCNTs were washed with distilled water until a neutral pH was reached. Sample G01 was prepared from the as-purified product and this was the starting material of the wet chemical and mechanochemical functionalization procedures, too. The wet chemical functionalization method consisted of two or three steps [27, 28]. The first step was an acidic treatment in HNO_3 or in HNO_3/H_2SO_4 mixture in order to form –COOH groups on the nanotube surface. In the next step, these carboxylic groups were transformed to –COCl groups by mixing the nanotubes in $SOCl_2$. Some of the samples were mixed in diaminopropane (DAP) as a third step (TEM image: Fig. 1b). The mechanochemical method [29, 30] was ball milling in reactive (NH_3, Cl_2, $COCl_2$, $SHCH_3$) atmospheres or in air. A typical TEM image of the CNT material ball milled in Cl_2 atmosphere can be seen in Fig. 1c, showing agglomerates of broken MWCNTs connected presumably by functional groups. The sample denoted by G11 was treated in the mixture of H_2SO_4 and $KMnO_4$ for 4 h after ball milling in order to remove the possible impurities from the mill and the amorphous carbon produced during milling [31]. G24 was annealed in pure N_2 gas at 1000°C temperature and 10^7 Pa pressure. The starting nanotube materials were ultrasonically treated in ethanol with a power of 350 W for 1 min, except for sample G15 which was processed for 6 min (in this case the nanotubes were connected to each other during functionalization [28]).

Random networks of nanotubes were formed by filtering the suspensions through polycarbonate membrane filters with 400-nm hole size. We formed circular dots from the nanotube layers with about 1.5-mm diameter with approximately uniform layer thickness (Fig. 2). The nanotube amount in the layers was about 0.6 μg/mm^2. In the case

Table 1 Preparation conditions of the CNT materials and sensing elements

Sample ID	Description	Ref.
G01	CCVD MWCNT, purified: NaOH and HCl	[23]
G02	Same as G01 and 3:1 H_2SO_4: HNO_3, $SOCl_2$ and DAP	[28]
G03	Same as G01 and HNO_3 and $SOCl_2$	[27]
G04	Same as G01 and HNO_3, $SOCl_2$ and DAP	[27]
G05	Same as G01 and 3:1 H_2SO_4: HNO_3 and DAP	[27]
G06	Same as G01 and ball milled in NH_3, 1 day	[29]
G07	Same as G01 and ball milled in Cl_2, 1 day	[29]
G08	Same as G01 and ball milled in $COCl_2$, 1 day	[29]
G09	Same as G01 and ball milled in $SHCH_3$, 1 day	[29]
G10	Same as G01 and ball milled in air, 1 day	[29]
G11	Same as G10 and H_2SO_4 and $KMnO_4$	
G12	Arc SWCNT grown in He, purified: HNO_3	[24]
G13	Arc MWCNT grown in He, purified: HNO_3	[25]
G14	Arc MWCNT grown under water	[26]
G15	Same as G01 and H_2SO_4: HNO_3, $SOCl_2$, DAP, ultrasonication 6 min	[28]
G16	Same as G01 and ball milled in NH_3, 4 days	[29]
G17	Same as G01 and ball milled in NH_3, 2 days	[29]
G18	Same as G04, thinner layer	[27]
G19	Same as G07, thinner layer	[29]
G20	Same as G08, thinner layer	[29]
G21	Same as G13, thinner layer	[25]
G22	Same as G01 and ball milled in NH_3, 14 h	[30]
G23	Same as G01 and ball milled in H_2S, 14 h	[30]
G24	Same as G01 and annealed: 1000 °C, 1 h, 100 bar N_2	

of samples G18–G21, we used thinner layers of 0.06 μg CNTs/mm^2 in order to obtain higher resistance and better signal to noise ratio. Sensor elements were prepared by contacting the nanotube layer dots by gold evaporation (Fig. 2). The middle of each dot was masked during gold deposition, resulting in an uncovered zone with approximately 1 mm^2 active area in between two gold covered stripes.

The chemical sensing properties of the samples were characterized by comparing the electrical resistance measured between the two gold stripes of each sensor exposed to air and to different gases and vapors. A special measuring electronics consisting of a current generator and a voltage amplifier were built, and the output was connected to a National Instruments PCI-6024E data acquisition card. Eight parallel channels were measured. Depending on the resistance of each sensor, the measuring current was chosen to be 1, 10 or 100 μA in order to reach the best possible voltage reading resolution. The resistance was found to be independent of the measuring current; the current–voltage curve was linear in the −1 to +1 mA range. The resistances of the sensors varied between 100 Ω and 10 MΩ. The resistance values were calculated from the fixed current and measured voltage values, using a sampling frequency of 10 Hz. The measurements were carried out at room temperature in streaming air (to which gases or vapors were added) driven by a membrane pump of 200 l/h capacity. The sensors were placed in a glass tube, the pump was connected to the output of the glass tube, while the air or air + vapor mixture was introduced through a flexible inlet tube of small diameter. The scheme of the measuring system is shown in Fig. 3. All the bottles containing the liquids used as vapor sources were of 1000 ml volume, 80 mm diameter and 30 mm neck diameter. They contained 100 ml of the liquid chemical to be tested and saturated vapor above the liquid. The measurements started by pumping ambient air through the system for 40–60 s, then the inlet was inserted in the bottle for 60 s and finally removed. The vapors of ethanol, acetone, toluene, water, pentane, xylene, trichloroethylene (TCE), butyl acetate, ammonia (0.25% solution in water) and chloroform were used for testing. The saturation concentration and the evaporation speed of these vapors are different; therefore, the behavior of the same sensors in the presence of different compounds can not directly be compared. However, the comparison of the responses of different sensors for the same vapor is correct since the course of the ambient concentration change was the same in each case because of the

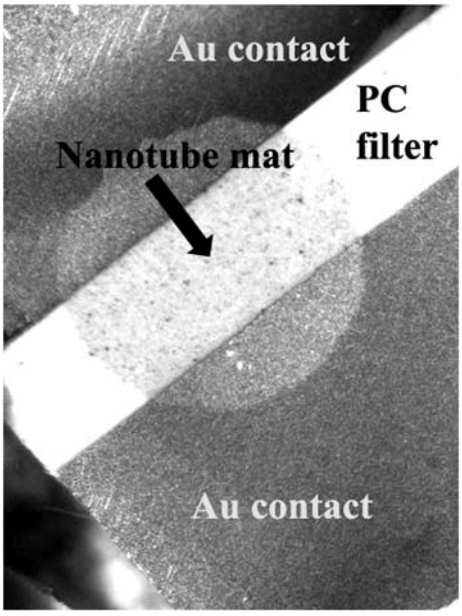

Fig. 2 Optical micrograph of a typical sensor element

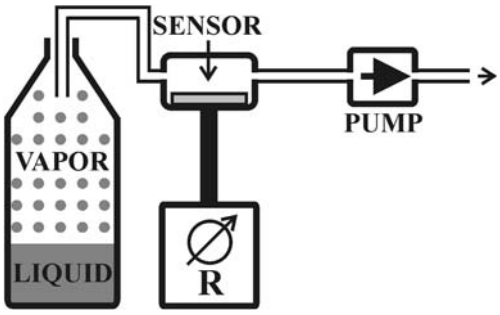

Fig. 3 Experimental setup of the measuring system

identical circumstances. The same set of sensors was used for all analytes, and the measurements were repeated several times. The sensors recovered within 5–10 min after exposure to most analytes, except for ammonia, in which case the recovery time exceeded one hour. We did not observe any degradation of the sensors after about 100 measurements.

In order to investigate the effect of the defects on the sensitivity and selectivity of the nanotubes, seven selected samples (see Table 3) were irradiated with Ar^+ ions of 30 keV, with a dose of 10^{13} ions/cm^2. After irradiation, the sensing properties of these sensors were characterized again in the same way.

3 Results

As examples, Fig. 4 shows the electrical responses, i.e. the relative resistances of samples G24, G01, G02 and G19, as a function of time when exposed to a mixture of air and vapors of ethanol, acetone, TCE and water. The relative resistance is calculated by dividing the actual resistance by the initial value measured in streaming ambient air. The first 60 s, when ambient air was flowed through the measuring tube, shows only slow changes in most cases. It is followed by an abrupt change of the signal when the tested vapor arrives. The response time of the system is only a few seconds, as shown in Fig. 4. This is practically the time needed for changing the ambient of the sensors; therefore, the reaction time of the sensors itself might even be shorter. The maxima of the relative resistance changes for all the tested sensor/vapor combinations are given in rounded percentages in Table 2. Zero means that the changes were below 0.5%. Nearly all the sensors are sensitive to all vapors but to a different degree. Some correlation of the overall signal strength with the vapor pressure of the compounds can be observed, but it is modified by specific interactions between vapors and sensors. The relative resistance curves when the sensors are exposed to acetone start with a peak followed by a quick decrease. This overshoot can be attributed to introducing saturated gas mixture first, while the acetone concentration decreases during the continuous flow. In the case of ethanol, TCE and all the organic solvents not shown here in detail, characteristics similar to the case of acetone can be observed; however, the changes in the resistance can be different. The measurements presented in the different segments of Fig. 4 were simultaneously recorded; therefore, the concentration of each vapor sensed by the different sensors can be regarded as identical. A 5-min regeneration time was left between two measurements; in some cases a slow decrease in the resistance can be observed in the first minute due to the incomplete desorption of the previous vapors. As for water, we found the majority of the sensors insensible. While there is no visible correlation between the sensitivity of the sensors for water and the organic solvents examined here, ammonia shows similar behavior to water. The first four sensors in the order of sensitivity for ammonia are the same for water (G12, G16, G02 and G11, respectively, see Table 2). The shape of the curves in the case of water also shows a different tendency, in contrast to the sharp peak at the beginning of the period when organic vapors are present. A quick increase and a quick decrease of the signal can be observed after the appearance and vanishing of the excess water vapor in the system, respectively. In between these, a plateau (see e.g. Fig. 4d) or a slower increase of the signal (Fig. 5d) is typical. Ammonia again behaves like water (not shown here), except that the amplitudes are typically much larger.

Comparing the overall sensitivity of the different sensors based on Table 2, we find that the least sensitive sensor is made of sample G24, the one annealed at elevated temperature and high pressure in pure N_2 atmosphere. The sensitivity of sensor G01 made of the raw, not intentionally functionalized CCVD grown MWCNT sample is higher than the

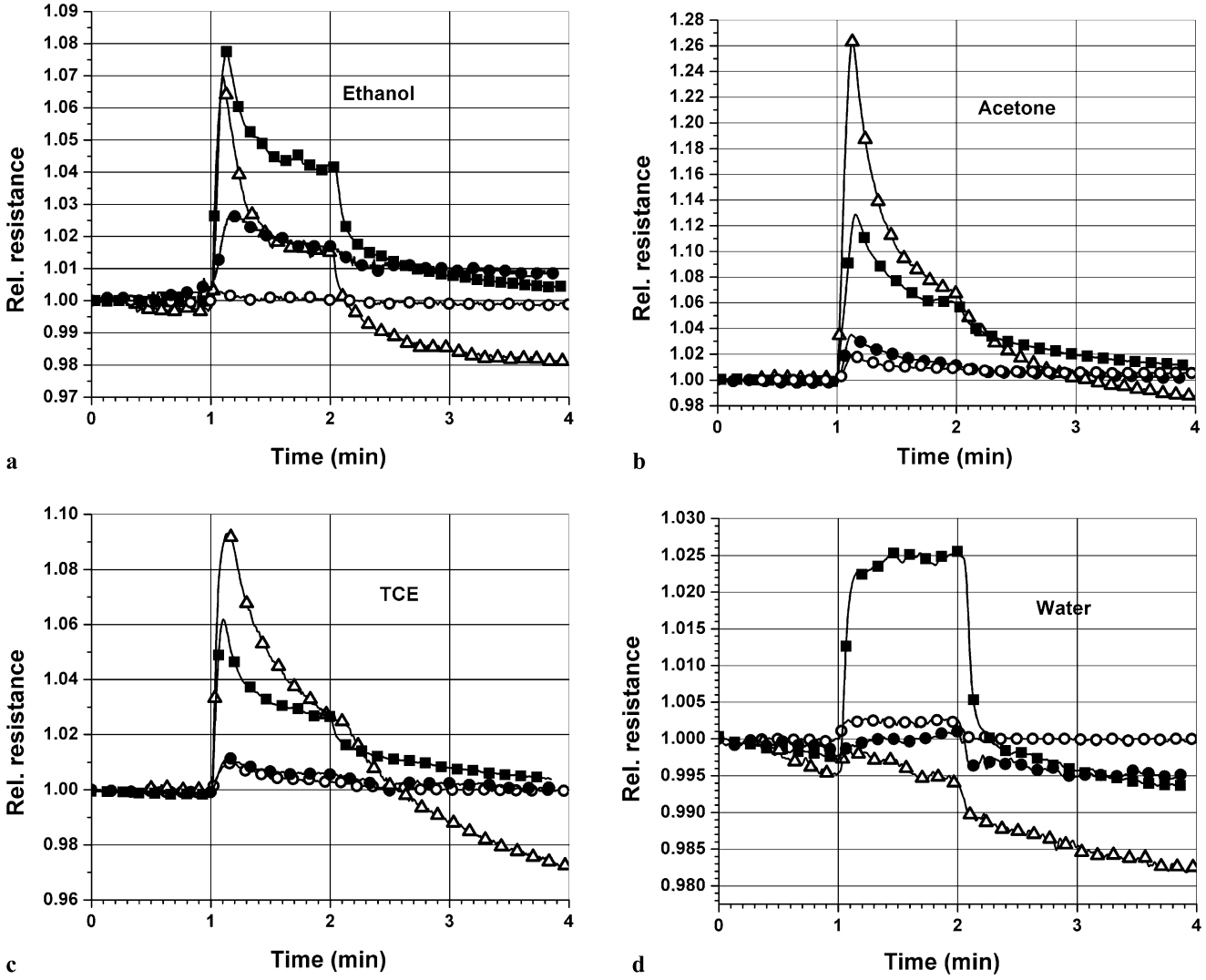

Fig. 4 Relative resistances of sensors G24 (○), G01 (●), G02 (■) and G19 (△) in streaming ethanol (**a**), acetone (**b**), TCE (**c**) and water (**d**) vapors, compared to ambient air. The analytes were pumped through the measuring system from 1 to 2 min

previously mentioned one but smaller than in the case of the functionalized sensors. The sensitivity of the other sensors shows a varied picture when exposed to the mentioned vapors; we can find individual differences in the sensitivities. All the catalytic CVD MWCNT samples ball milled for one day (G06–G11, G19 and G20) give good overall sensitivity, even if processed in non-reactive atmosphere like G10. However, comparing the responses of G11 to G10, we can see an enhanced sensitivity especially for acetone, water, pentane, ammonia and TCE. These two samples were ball milled in the same way in air, but, after it, G11 was subjected to selective oxidation in the solution of sulfuric acid and potassium permanganate.

Another comparison can be made based on the ball milling duration: two samples, G22 and G23, ball milled only for 14 h in NH_3 and H_2, respectively, showed rather similar behavior but definitely weaker sensitivity than all the other ball milled samples. Longer milling up to a certain time can enhance sensitivity, depending on the studied vapor. Especially, in the set of G22, G06, G17 and G16, ball milled in ammonia ambient for 14 h, 1, 2 and 4 days, respectively, the sensitivity for water, TCE and ammonia grew monotonically with increasing milling time. For the other compounds, maximum sensitivity was achieved at shorter milling times.

Based on their overall sensing behavior, the samples functionalized using wet chemistry (G02, G04, G05, G15 and G18) do not differ significantly from ball milled samples. However, the samples treated first in the more reactive oxidizing agent [27], a mixture of nitric and sulfuric acids (G02, G05 and G15) and not only in nitric acid (G04 and G18), show usually higher sensitivities.

Three of the sensors (G12, G13 and G14) were made of different arc-grown nanotube materials. None of these mate-

Table 2 Maximum values of the relative resistance changes for all the measured sensor/vapor combinations in percentage

Sample ID	Ethanol	Acetone	Toluene	Water	Pentane	Xylene	Trichlor-ethylene	Butyl acetate	Ammonia 0.25%	Chloroform
G01	2	3	0	0	4	0	1	0	3	1
G02	10	10	1	3	8	1	5	1	23	2
G03	2	0	0	0	3	0	0	0	0	2
G04	3	3	1	0	5	1	2	0	4	1
G05	5	10	1	1	17	1	4	1	5	2
G06	8	14	2	0	14	1	4	1	1	3
G07	7	17	2	0	15	1	4	1	0	4
G08	10	10	0	0	13	0	4	0	8	5
G09	6	15	4	0	5	2	5	1	2	7
G10	5	7	1	0	7	1	3	1	4	3
G11	6	11	1	3	16	0	7	1	16	1
G12	6	9	1	9	1	1	7	2	160	1
G13	11	12	4	0	12	3	7	1	6	9
G14	11	38	4	0	5	2	13	3	8	14
G15	10	17	1	2	6	1	6	1	10	3
G16	9	9	1	7	7	1	7	1	28	1
G17	10	13	1	2	7	1	5	1	8	3
G18	5	8	2	0	5	1	3	1	3	3
G19	6	26	7	0	6	3	9	2	1	12
G20	9	18	3	0	8	1	5	1	5	4
G21	11	22	2	1	10	2	6	2	5	5
G22	2	4	2	0	2	1	3	1	1	4
G23	2	4	2	0	2	1	2	1	1	4
G24	0	1	0	0	1	0	1	0	1	0

rials were purposely functionalized, but G12 and G13 were purified by an acidic treatment in nitric acid [25]. The overall picture of the sensitivity of the two arc-grown MWCNT samples is similar, and they do not substantially differ from the CCVD samples, though sensor G14 shows the highest sensitivity for acetone, TCE, butyl acetate and chloroform and one of the best for ethanol and xylene. G12, the only sensor made of SWCNTs, shows a somewhat different behavior; it gives an extremely high signal for ammonia, more than five times larger than any of the others. Besides, it is the most sensitive for water, but this sensitivity is not as protruding as in the case of ammonia. Another characteristic feature of G12 is that in contrast to these, it has as low response for pentane as the least sensitive sensor, G24.

Not only the nanotube material preparation, but also the sensor preparation parameters, can affect the sensitivity. The duration of ultrasonication was different, one minute and six minutes in the cases of G02 and G15, respectively. Comparing their sensitivities, no general tendency can be observed, though remarkable differences are present: increase in case of acetone and decrease in case of ammonia. The effect of the nanotube layer thickness was studied in the case of four different CNT materials, using one-tenth of the usually applied amount of material for layer preparation in the case of the thinner layers. The sensor pairs with thicker and thinner layers were G04–G18, G07–G19, G08–G20 and G13–G21, respectively. Comparing their responses for the different vapors, a common trend can only be found in the case of acetone, showing increased sensitivity of the thinner layers; otherwise, the difference in layer thickness either has no significant effect or changes with opposite senses can be observed.

The relative changes of the resistances due to Ar^+ irradiation as well as the maximum values of the relative resistance changes of the raw and irradiated sensors are shown in Table 3. The resistances measured in air increased by less than 20% for G01, G09 and G24, while they decreased by less than 20% for G02 and G19, respectively. A more significant resistance decrease was detected for G14 made of arc-grown MWCNTs. The resistance increased dramatically, two and a half times, in the case of sensor G12 made of SWCNTs. Comparing the resistance changes for the measured 70 sensor/vapor combinations, we can conclude that in most cases the sensitivity of the detectors decreased as

Table 3 The relative resistance changes caused by irradiation and comparison of the maximum values of the relative resistance changes of the irradiated (irr) and raw samples in percentage

Sample ID	$(R_{ir} - R_{raw})/R_{raw}$ (%)	Ethanol		Acetone		Toluene		Water		Pentane		Xylene		Trichlor-ethylene		Butyl acetate		Ammonia 0.25%		Chloro-form	
		irr	raw	irr	raw	irr	raw	irr	raw	irr	raw	irr	raw	irr	raw	irr	raw	irr	raw	irr	raw
G01	17	1	2	2	3	0	0	0	0	0	4	0	0	0	1	0	0	1	3	0	1
G02	−16	4	10	5	10	0	1	1	3	0	8	0	1	0	5	0	1	10	23	1	2
G09	17	2	6	20	15	0	4	0	0	6	5	0	2	2	5	0	1	0	2	2	7
G12	253	1	6	3	9	0	1	6	9	−1	1	−2	1	0	7	−2	2	170	160	0	1
G14	−37	6	11	44	38	1	4	0	0	3	5	0	2	6	13	0	3	5	8	6	14
G19	−19	4	6	9	26	0	7	0	0	1	6	0	3	1	9	0	2	0	1	1	12
G24	19	0	0	0	1	0	0	0	0	0	1	0	0	0	1	0	0	1	1	0	0

an effect of irradiation. There are only four exceptions from this rule: G09 and G14 are more sensitive to acetone, G12 to ammonia and G09 to pentane after irradiation, but the change in all the four cases is only moderate while in some of the other cases the sensitivity decreased from a remarkable value down to zero, see e.g. G19 for toluene, G02 for pentane and G12 for TCE. Irradiation was most destructive for the sensing of toluene and xylene; almost all the sensors became insensible. In the case of sensor G12 made of arc-grown SWCNTs, irradiation induced a reversed functioning in the presence of pentane, xylene and butyl acetate: the sensor resistance decreased in the presence of these vapors.

Time-dependent behavior of the raw and irradiated sensors in a few typical cases (G01 and G14 for acetone, G02 for ethanol and G12 for water) is presented in Fig. 5. As can be seen, not only the amplitude of the signals but the shape of the curves has been changed because of the irradiation. Typically, the curves of the irradiated sensors show slower changes: the peaks are more rounded and the signals decrease much more slowly after the vapor feedstock is turned off. Anyway, the different behavior of the sensors with a starting peak in the case of organic solvents and with a plateau or slow increase in the medial period in the case of water and ammonia was preserved.

4 Discussion

The resistance changes of semiconducting CNTs are explained by the charge transfer between the nanotube and the adsorbed molecules [13, 32]. However, the case of metallic CNTs is much less discussed, especially if different functional groups are attached to their surfaces. Although the precise mechanism is not known, we may suppose that the change of the conductivity of the CNTs is due to increased scattering due to weakly adsorbed molecules on the CNT surface, or at the CNT–CNT junctions, as was suggested by Esen et al. [16]. The varied picture of sensing behavior of differently treated sensor materials in the case of the applied gases/vapors is the consequence of the specific and collective adsorption/desorption and electronic properties of each nanotube–defect site(s)–attached functional group(s)–adsorbed molecule(s) system present in the sensors. The role of the different defects as adsorption sites has already been discussed in a few specific cases [5, 8–10, 12, 13], but much more work is still needed for a comprehensive description of the topic. In air, a part of the adsorption sites can be occupied [6]; therefore, besides the compound to be sensed, the effect of the species present in the air must also be taken into consideration. This makes the understanding of the sensing mechanism in most of the practical cases even more complicated. However, the differences in the response including the time dependence of the signal offer a possibility for selective gas sensing. Though none of the sensors can individually be applied as an exclusively selective sensor for any of the investigated chemicals, the 'fingerprint' of a vapor, i.e. the response of a set of selected sensors, can be characteristic for a gas or vapor. For the demonstration of this, we have built a vapor recognition device made of sensors G09, G12, G14 and G19 developed for the identification of water, ethanol, acetone, chloroform and TCE. After a teaching process, in which the resistance change of each mentioned sensor as a function of time is recorded for all the five mentioned vapors, the device is able to identify one of the mentioned five if the measurement conditions are the same as during teaching. The identification is based simply on the comparison of the response of the unknown vapor with the previously recorded ones and the choice of the best fitting one; see details in [33].

In the case of our sensors made of functionalized catalytic CVD MWCNT samples, the correlation of the overall sensitivity with the duration or strength of the applied defect

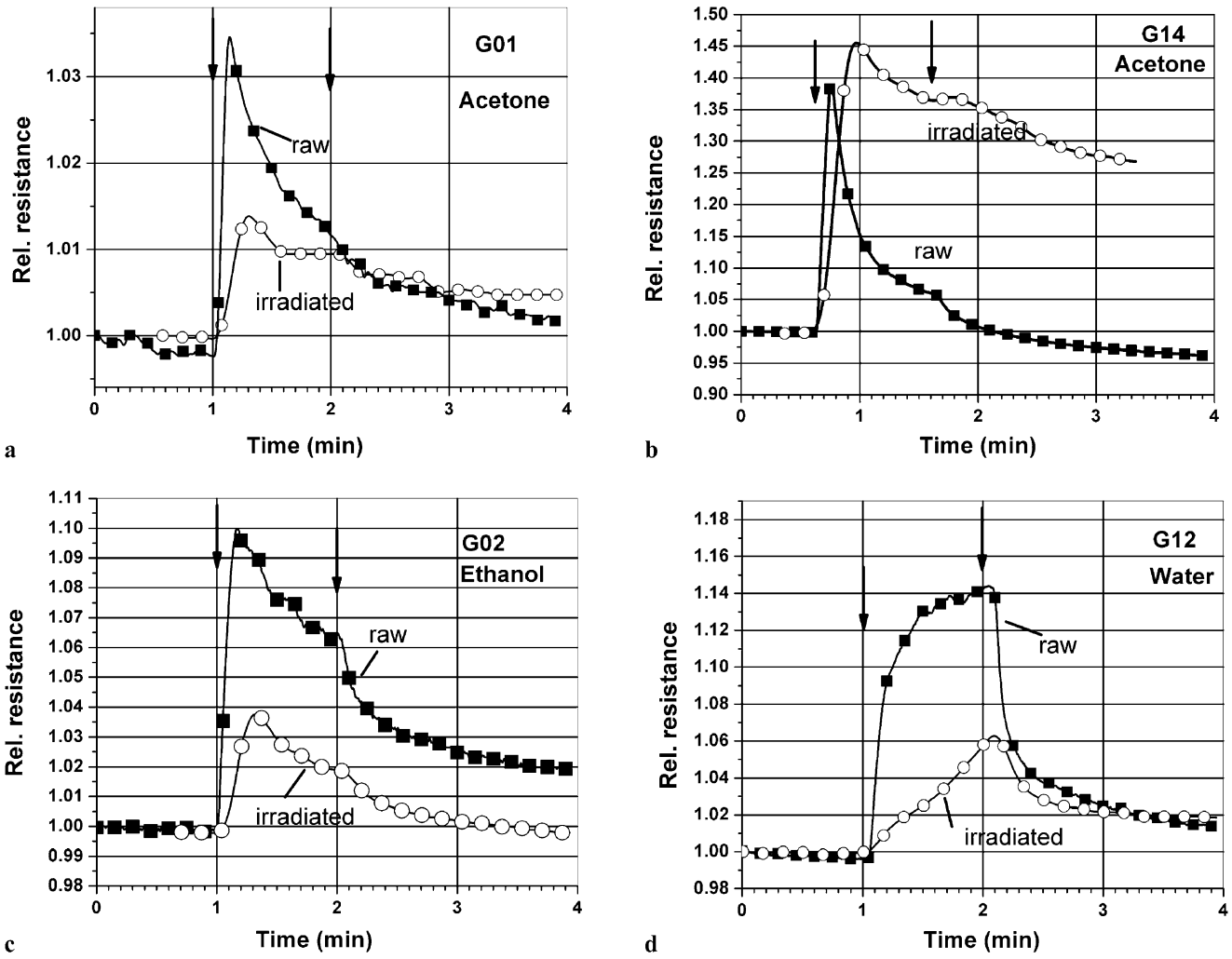

Fig. 5 Comparison of relative resistances of raw and irradiated (Ar^+ ions, 30 keV, 10^{13} ions/cm^2) sensors in the case of four selected sensor/vapor combinations: (**a**) G01/acetone, (**b**) G14/acetone, (**c**) G02/ethanol, (**d**) G12/water. The start and the end of the analyte vapor pumping through the sensing system are denoted by *arrows*

generating processes, i.e. the ball milling and chemical oxidation, can clearly be seen. In case of the G10/G11 sensor pair, the enhanced sensitivity of G11 can be explained by the additional oxidation of the defected regions caused by the purification in H_2SO_4/$KMnO_3$ mixture solution. A similar treatment was used by Hiura et al. for the removal of amorphous carbon and the opening of carbon nanotubes [31].

On the other hand, sensor G24 shows a smaller effect than sensor G01 made of raw MWCNT material. The presence of functional groups attached to the surface of similar, purified nanotubes was demonstrated by Ötvös et al. [34]. Annealing in pure N_2 atmosphere can partially heal the structural defects [22] and remove functional groups anchored to these defects. All these facts are in accordance with the picture that functional groups can act as active sites in the sensing mechanism. We can suppose that the larger the number of functional groups (up to a certain value), the stronger the effect of gas/vapor molecules on the conductivity of the CNTs. Arc-grown carbon nanotubes are known to contain much fewer structural defects than CVD-grown ones. Considering the good overall sensitivity of the sensors G12, G13 and G14, we could assume at first sight that the above-mentioned correlation of the sensitivity with the defect density is not valid in case of our arc-grown MWCNT and SWCNT samples. However, though it was not investigated here in detail, the presence of a significant number of functional groups can be assumed due to the acidic purification in the case of the starting material of G12 and G13 and the special, reactive growth ambient of G14. Besides, arc-grown MWCNTs are much shorter than CVD-grown ones, so the density of tube ends in these samples is higher. Tube ends can be considered as defect sites of the perfect hexagonal network, they are more reactive than the tube walls [35],

so functional groups can be linked here with higher probability.

The effects of the irradiation treatment can be compared to ball milling: though defects are generated in both cases, irradiation decreased the sensitivity in most cases, while ball milling even in non-reactive air ambient caused significant improvement. It is expected that irradiation induced partial destruction of the bonds in the outer graphitic layer causes the significant increase of the resistance of the sensors, as happens in the case of G12, the sensor made of SWCNTs. In the case of the other, MWCNT-made sensors, however, only moderate changes, including both increase and decrease of the resistance, were observed. This can be the consequence of another, competing effect: the formation of bonds between the layers of MWCNTs. (The structural effects of such irradiation on CNTs were investigated in detail elsewhere [22].) In perfect MWCNTs, mostly the outermost wall is responsible for the conduction [4]. Covalent bonding between the layers can cause the increase of the contribution of inner walls in the electrical transport. This can compensate the effect of higher defect density on the conductivity. On the other hand, if a higher part of the current is not directly affected by the surface conditions, the drop of the sensor sensitivity can be expected, as we indeed observed in most of the cases. In the case of SWCNTs, such a plausible explanation cannot be found, but the effect of the structural changes implied by the significant increase of the resistance seems to be more destructive; the resulting electronic structure is much less similar to the graphitic one. Another difference in the defect generation process conditions possibly relevant in respect to chemical sensing is that ion irradiation has been carried out in vacuum. The lack of foreign molecules made possible the relaxation of irradiation-caused dangling bonds mostly by C–C connections. The attachment of foreign atoms or functional groups is much less probable than during growth, ball milling or wet chemical treatment, including purification.

5 Conclusion

As the outer wall of the carbon nanotube plays a dominant role in the electrical transport along the axis [4], the influence of the ambient on its electrical properties offers the possibility of chemical sensing. In our work, the modification of electrical conduction was used as the detection principle in random networks of carbon nanotubes made mostly of differently treated CVD-grown MWCNTs. A sensor made of arc-grown SWCNTs and two others made of arc-grown MWCNTs were also investigated. The response of 24 different sensors to 10 vapors was studied. CNT networks exhibited less than 10-s response times to all vapors applied. The average sensitivity of the sensors was found to be increasing with the number of attached functional groups while the individual sensitivity of the different sensors showed a varied picture depending on the preparation conditions. Ar^+-ion irradiation caused in most cases the decrease of the sensitivity in contrast to other defect generation methods such as acidic oxidation and ball milling. The sensors were not exclusively selective to only one investigated chemical, but the differences in the individual sensitivities and in the time-dependent response curves give opportunity to the recognition of various chemicals using properly selected sets of different sensors.

Acknowledgement Financial support of the Hungarian Scientific Research Fund (OTKA) under grants T049182, OTKA–NKTH-NI67851, K67793 and the project MTA-MEH 'Nanogas' is acknowledged. One of the authors (Z.E.H.) is a grantee of a Bolyai János Scholarship.

References

1. S. Iijima, Nature **354**, 56 (1991)
2. M.S. Dresselhaus, G. Dresselhaus, R. Saito, Carbon **33**, 883 (1995)
3. J. Zhao, A. Buldum, J. Han, J.P. Lu, Nanotechnology **13**, 195 (2002)
4. A. Bachtold, C. Strunk, J.P. Salvetat, J.M. Bonard, L. Forro, T. Nussbaumer, C. Schonenberger, Nature **397**, 673 (1999)
5. F. Mercuri, A. Sgamellotti, Inorg. Chim. Acta **360**, 785 (2007)
6. H. Ulbricht, R. Zacharia, N. Cindir, T. Hertel, Carbon **44**, 2931 (2006)
7. J. Andzelm, N. Govind, A. Maiti, Chem. Phys. Lett. **421**, 58 (2006)
8. X. Feng, S. Irle, H. Witek, K. Morokuma, R. Vidic, E. Borguet, J. Am. Chem. Soc. **127**, 10533 (2005)
9. J.A. Robinson, E.S. Snow, S.C. Badescu, T.L. Reinecke, F.K. Perkins, Nano Lett. **6**, 1747 (2006)
10. M. Grujicic, G. Cao, R. Singh, Appl. Surf. Sci. **211**, 166 (2003)
11. H. Hiura, T.W. Ebbesen, J. Fujita, K. Tanigaki, T. Takada, Nature **367**, 148 (1994)
12. N. Chakrapani, Y.M. Zhang, S.K. Nayak, J.A. Moore, D.L. Carroll, Y.Y. Choi, P.M. Ajayan, J. Phys. Chem. B **107**, 9308 (2003)
13. J. Kong, N.R. Franklin, C. Zhou, M.G. Chapline, S. Peng, K. Cho, H. Dai, Science **287**, 622 (2000)
14. M. Arab, F. Picaud, M. Devel, C. Ramseyer, C. Girardet, Phys. Rev. B **69**, 165401 (2004)
15. L. Hu, D.S. Hecht, G. Grüner, Nano Lett. **4**, 2513 (2004)
16. G. Esen, M.S. Fuhrer, M. Ishigami, E.D. Williams, Appl. Phys. Lett. **90**, 123510 (2007)
17. H.Q. Nguyen, J.S. Huh, Sens. Actuators B Chem. **117**, 426 (2007)
18. K. Parikh, K. Cattanach, R. Rao, D.S. Suh, A. Wu, S.K. Manohar, Sens. Actuators B Chem. **113**, 55 (2006)
19. O.K. Varghese, P.D. Kichambre, D. Gong, K.G. Ong, E.C. Dickey, C.A. Grimes, Sens. Actuators B Chem. **81**, 32 (2001)
20. L. Valentini, C. Cantalini, I. Armentano, J.M. Kenny, L. Lozzi, S. Santucci, Diam. Relat. Mater. **13**, 1301 (2004)
21. D. Bom, R. Andrews, D. Jacques, J. Anthony, B.L. Chen, M.S. Meiers, J.P. Selengue, Nano Lett. **2**, 615 (2002)
22. Z. Osváth, G. Vértesy, L. Tapasztó, F. Wéber, Z.E. Horváth, J. Gyulai, L.P. Biró, Phys. Rev. B **72**, 045429 (2005)
23. A. Kukovecz, Z. Kónya, N. Nagaraju, I. Willems, A. Tamasi, A. Fonseca, J.B. Nagy, I. Kiricsi, Phys. Chem. Chem. Phys. **2**, 3071 (2000)

24. C. Journet, W.K. Maser, P. Bernier, A. Loiseau, M. Lamy de la Chapelle, S. Lefrant, P. Deniard, R. Lee, J.E. Fischer, Nature **388**, 756758 (1997)
25. M.T. Martínez, M.A. Callejas, A.M. Benito, M. Cochet, T. Seeger, A. Ansón, J. Schreiber, C. Gordon, C. Marhic, O. Chauvet, J.L.G. Fierro, W.K. Maser, Carbon **41**, 2247 (2003)
26. L.P. Biró, Z.E. Horváth, L. Szalmás, K. Kertész, F. Wéber, G. Juhász, G. Radnóczi, J. Gyulai, Chem. Phys. Lett. **372**, 399 (2003)
27. K. Niesz, A. Siska, I. Vesselényi, K. Hernádi, D. Méhn, G. Galbács, Z. Kónya, I. Kiricsi, Catal. Today **76**, 3 (2002)
28. A.A. Koós, Z.E. Horváth, Z. Osváth, L. Tapasztó, K. Niesz, Z. Kónya, I. Kiricsi, N. Grobert, M. Rühle, L.P. Biró, Mater. Sci. Eng. C **23**, 1007 (2003)
29. Z. Kónya, I. Vesselényi, K. Niesz, Á. Kukovecz, A. Demortier, A. Fonseca, J. Delhalle, Z. Mekhalif, J.B. Nagy, A.A. Koós, Z. Osváth, A. Kocsonya, L.P. Biró, I. Kiricsi, Chem. Phys. Lett. **360**, 429 (2002)
30. I. Vesselényi, A. Siska, D. Méhn, K. Niesz, Z. Kónya, J.B. Nagy, I. Kiricsi, J. Phys. IV **12**, 107 (2002)
31. H. Hiura, T.W. Ebbesen, K. Tanigaki, Adv. Mater. **7**, 275 (1995)
32. S. Santucci, S. Picozzi, F. Di Gregorio, L. Lozzi, C. Cantalini, L. Valentini, J.M. Kenny, B. Delley, J. Chem. Phys. **119**, 10904 (2003)
33. Z.E. Horváth, A.A. Koós, K. Kertész, Z. Vértesy, G. Molnár, M. Ádám, C. Dücső, J. Gyulai, L.P. Biró, Nanopages **1**, 209 (2006)
34. Zs. Ötvös, Gy. Onyestyák, J. Valyon, I. Kiricsi, L.V.C. Rees, Stud. Surf. Sci. Catal. **156**, 617 (2005)
35. J.-C. Charlier, Acc. Chem. Res. **35**, 1063 (2002)